JGV Papers in Press. Published June 19, 2013 as doi:10.1099/vir.0.052910-0

VIR/2013/052910 - REVISED VERSION

MERS-coronavirus replication induces severe in vitro cytopathology and is strongly inhibited by cyclosporin A or interferon-alpha treatment

Adriaan H. de Wilde[1], V. Stalin Raj[2], Diede Oudshoorn[1], Theo M. Bestebroer[2], Stefan van Nieuwkoop[2], Ronald W. A. L. Limpens[3], Clara C. Posthuma[1], Yvonne van der Meer[1], Montserrat Bárcena[3], Bart L. Haagmans[2], Eric J. Snijder[1*] and Bernadette G. van den Hoogen[2*]

[1]Molecular Virology Laboratory, Department of Medical Microbiology, Leiden University Medical Center, Leiden, The Netherlands

[2]Viroscience Lab, Erasmus MC, Rotterdam, The Netherlands

[3]Section Electron Microscopy, Department of Molecular Cell Biology, Leiden University Medical Center, Leiden, The Netherlands

* Corresponding authors: Eric. J. Snijder (E.J.Snijder@lumc.nl) and Bernadette G. van den Hoogen (b.vandenhoogen@erasmusmc.nl)

Abstract word count: 235

Text word count: 5499

Number of figures: 7

Running title: MERS-CoV replication and sensitivity to CsA and IFN-α

Contents Category: Animal Viruses - Positive-strand RNA

SUMMARY

Coronavirus (CoV) infections are commonly associated with respiratory and enteric disease in humans and animals. The 2003 outbreak of severe acute respiratory syndrome (SARS) highlighted the potentially lethal consequences of CoV-induced disease in humans. In 2012, a novel CoV (Middle East Respiratory Syndrome coronavirus; MERS-CoV) emerged, causing 49 human cases thus far, of which 23 had a fatal outcome. In this study, we characterized MERS-CoV replication and cytotoxicity in human and monkey cell lines. Electron microscopy of infected Vero cells revealed extensive membrane rearrangements, including the formation of double membrane vesicles and convoluted membranes, which were previously implicated in the RNA synthesis of SARS-CoV and other CoVs. Following infection, we observed rapidly increasing viral RNA synthesis and release of high titres of infectious progeny, followed by pronounced cytopathology. These characteristics were used to develop an assay for antiviral compound screening in 96-well format, which was used to identify cyclosporin A as an inhibitor of MERS-CoV replication in cell culture. Furthermore, MERS-CoV was found to be 50-100 times more sensitive to interferon-alpha (IFN-α) treatment than SARS-CoV, an observation that may have important implications for the treatment of MERS-CoV-infected patients. MERS-CoV infection did not prevent the IFN-induced nuclear translocation of phosphorylated STAT1, in contrast to infection with SARS-CoV where this block inhibits the expression of antiviral genes. These findings highlight relevant differences between these distantly related zoonotic CoVs in terms of their interaction with and evasion of the cellular innate immune response.

51 **INTRODUCTION**

52

53 In June 2012, a previously unknown coronavirus was isolated from a 60 year-old Saudi-
54 Arabian patient who died from acute respiratory distress syndrome and multiple organ failure (Zaki *et*
55 *al.*, 2012). Subsequently, the novel virus was isolated from several additional residents and visitors of
56 the Arabian Peninsula suffering from similar respiratory symptoms. In retrospect, also a cluster of
57 respiratory infections in Jordan (April 2012) was linked to the same agent, although no convincing
58 evidence for human-to-human transmission was obtained. This was clearly different for a cluster of
59 three U.K. cases in early 2013, consisting of a patient who had travelled to Saudi Arabia and two
60 family members without recent travel history outside the U.K. In the past year, various names have
61 been used to refer to this newly identified CoV, including novel (beta)coronavirus (nCoV) and human
62 coronavirus EMC (HCoV-EMC), but following a recent recommendation by the coronavirus study
63 group of ICTV and other experts (de Groot *et al.*, 2013) we will use Middle East Respiratory
64 Syndrome coronavirus (MERS-CoV) throughout this paper. Up to May 2013, 49 confirmed MERS
65 cases, including 23 fatalities, have been recorded
66 (http://www.who.int/csr/don/archive/disease/coronavirus_infections/en/).

67 Coronavirus (CoV) infections are associated with respiratory and enteric disease in humans
68 and animals. Since the 1960s, two human CoVs (HCoVs OC43 and 229E) were known to cause mild
69 respiratory disease (Hamre & Procknow, 1966; McIntosh *et al.*, 1967), but it was the 2003 outbreak of
70 severe acute respiratory syndrome (SARS; fatality rate ~10%) that revealed the potentially lethal
71 consequences of CoV-induced disease in humans (Drosten *et al.*, 2003; Ksiazek *et al.*, 2003). Two
72 years later, bats were identified as the most likely animal reservoir for this zoonotic CoV (Lau *et al.*,
73 2005; Li *et al.*, 2005). Subsequently, a wide variety of bat-associated CoVs was discovered
74 (Vijaykrishna *et al.*, 2007; Woo *et al.*, 2007) and also two additional human CoVs (NL63 and HKU1;
75 (Fouchier *et al.*, 2004; van der Hoek *et al.*, 2004; Woo *et al.*, 2005) were identified. Although the
76 general capacity of bat CoVs to switch hosts appears to be rather restricted (Muller *et al.*, 2012), the

77 possibility of SARS-CoV re-emergence or zoonotic transfer of other animal CoVs has remained a
78 public health concern over the past 10 years.

79 Coronaviruses are classified in four genera (alpha-, beta-, gamma- and deltacoronaviruses; (de
80 Groot *et al.*, 2012) and our previous analysis of the MERS-CoV genome (van Boheemen *et al.*, 2012)
81 identified the newly emerging agent as a member of lineage C of the genus *Betacoronavirus*.
82 Strikingly, as in the case of SARS-CoV, the closest known relatives of MERS-CoV are bat
83 coronaviruses, like HKU-4 and HKU-5(van Boheemen *et al.*, 2012; Woo *et al.*, 2007). The
84 evolutionary distance to SARS-CoV (lineage B) is considerable, a notion further supported by recent
85 comparative studies revealing important differences in receptor usage (Muller *et al.*, 2012; Raj *et al.*,
86 2013).

87 Mammalian viruses have to cope with the host cell's innate responses, including those
88 triggered by activation of the type I interferon (IFN) pathway (reviewed by (Randall & Goodbourn,
89 2008). Coronaviruses, including SARS-CoV, appear to have evolved a variety of mechanisms to
90 block or evade such antiviral responses (reviewed in (Perlman & Netland, 2009; Zhong *et al.*, 2012).
91 For example, it was postulated that the sensing of double-stranded (ds) RNA replication intermediates
92 by the innate immune system is inhibited by the elaborate virus-induced membrane structures with
93 which CoV RNA synthesis is associated (Knoops *et al.*, 2008; Versteeg *et al.*, 2007). Other evasion
94 mechanisms were attributed to protein functions that can be either conserved across CoVs or specific
95 for certain CoV lineages. Proteins such as the nsp3 proteinase (Ratia *et al.*, 2006), the nsp16 2'-O-
96 methyltransferase (Zust *et al.*, 2011), and the products of SARS-CoV ORFs 3b, 6 and 7a (Frieman *et*
97 *al.*, 2007; Hussain *et al.*, 2008; Kopecky-Bromberg *et al.*, 2006; Zhou *et al.*, 2012) have all been
98 described to prevent IFN induction/signalling. In particular, the SARS-CoV ORF6 protein is known to
99 inhibit IFN-induced JAK-STAT signalling by blocking the nuclear translocation of phosphorylated
100 STAT1 (p-STAT1), which contributes to the pathogenic potential of the virus in a mouse model (Sims
101 *et al.*, 2013). In spite of these immune evasion strategies, treatment with type I IFNs can inhibit CoV
102 replication *in vitro* (Garlinghouse *et al.*, 1984; Haagmans *et al.*, 2004; Paragas *et al.*, 2005; Taguchi &
103 Siddell, 1985; Zheng *et al.*, 2004) and, for example, protected type I pneumocytes against SARS-CoV
104 infection in macaques (Haagmans *et al.*, 2004).

105 Clearly, well-characterized systems for MERS-CoV replication in cell culture will be
106 invaluable for future studies into basic virus properties and interactions with the host, including innate
107 immune responses. Therefore, we set out to characterize the replication of MERS-CoV in different
108 cell lines. Using this information, an assay to screen for antiviral compounds was developed, which
109 identified cyclosporin A (CsA) as an inhibitor of MERS-CoV replication. Our first screening
110 experiments also established that, compared to SARS-CoV, MERS-CoV replication is more sensitive
111 to type I interferon treatment.
112
113 **RESULTS**
114
115 **Kinetics of MERS-CoV replication in Vero and Huh7 cells.** Only a few laboratory studies on
116 MERS-CoV replication have been reported thus far. Cells from a variety of mammalian hosts were
117 found to be susceptible and infection can induce pronounced cytopathology and cell death (Muller *et*
118 *al.*, 2012; Zaki *et al.*, 2012). Following entry, the CoV replicative cycle starts with the translation of
119 the positive-stranded RNA genome into replicase polyproteins that are cleaved into 16 nsps
120 (Gorbalenya *et al.*, 2006; van Boheemen *et al.*, 2012). These direct both genome replication and the
121 synthesis of the subgenomic (sg) mRNAs required to express the structural and accessory proteins. To
122 investigate MERS-CoV replication in more detail, we used Vero and Huh7 cells to analyse viral RNA
123 synthesis and progeny release in single-cycle infection experiments.
124 Hybridisation analysis of the accumulation of viral RNA revealed the presence of genome
125 RNA and seven sg transcripts, with sizes closely matching those previously predicted from the
126 positions of conserved transcription regulatory sequences (TRS) in the viral genome (van Boheemen
127 *et al.*, 2012) (Fig. 1a). The relative abundance of the various sg mRNAs is similar to what has been
128 observed for other CoVs, with the smallest species (encoding the N protein) being by far the most
129 abundant transcript (Fig. 1b). In both cell lines, viral mRNAs could be readily detected at 7 h p.i. and
130 reached maximum levels around 13 h p.i. (Fig. 1a). Viral RNA levels remained more or less constant
131 until 24 h p.i. in Vero cells, whereas the amount isolated from Huh7 cells declined due to the more
132 rapid development of cytopathology in this cell line between 13 and 24 h p.i. (see below). After the

133 peak of viral RNA accumulation had been reached, the titre of virus released from MERS-CoV-
134 infected Vero cells steadily increased from ~5 x 10^5 to ~5 x 10^7 p.f.u. per ml (Fig. 1c). Interestingly,
135 the bulk of the viral progeny was released significantly earlier from Huh7 cells, although the final titre
136 at 24 h p.i. was comparable to that obtained from Vero cells.
137
138 **Antisera raised against non-structural proteins of other betacoronaviruses cross-react with**
139 **MERS-CoV proteins.** Despite the relatively large evolutionary distance to better-characterized
140 CoVs, we tested a panel of antisera from our laboratory for cross-reactivity with MERS-CoV-infected
141 cells. In contrast to a polyclonal serum recognizing the SARS-CoV nucleocapsid (N) protein (data not
142 shown), antisera against various SARS-CoV nsps (nsp3, nsp5, nsp8; (Snijder *et al.*, 2006) raised using
143 purified recombinant proteins as antigen, were found to strongly cross-react (Fig. 2a). In addition,
144 rabbit antisera raised against synthetic peptides (23-mers) representing a small but conserved C-
145 terminal part of SARS-CoV and MHV nsp4 strongly cross-reacted with MERS-CoV. Only small but
146 apparently immunogenic parts of these peptides (*e.g.*, LYQPP) are absolutely conserved between
147 MHV and MERS-CoV nsp4 (Fig. 2b). Conservation in other betacoronaviruses (data not shown)
148 suggests that antisera recognizing this nsp4 region may be used for immunodetection of additional
149 (newly emerging) CoVs.
150
151 **MERS-CoV replication structures.** Subsequently, we employed a monoclonal antibody recognizing
152 dsRNA to localize intermediates in viral RNA synthesis (Knoops *et al.*, 2008; Weber *et al.*, 2006). In
153 various cell types, the immunolabelling signals for both replicase and dsRNA localized to the
154 perinuclear region (Fig. 2c), where the replication structures induced by other CoVs are known to
155 accumulate (Brockway *et al.*, 2003; Gosert *et al.*, 2002; Knoops *et al.*, 2008; Snijder *et al.*, 2006;
156 Stertz *et al.*, 2007; Ulasli *et al.*, 2010).
157 We next used electron microscopy (EM) to investigate the ultra-structural and potentially
158 cytopathic changes that MERS-CoV induces in infected cells, and focused on the membranous
159 replication structures that support MERS-CoV RNA synthesis. The preservation of such structures,
160 typically double-membrane vesicles (DMVs) and convoluted membranes (CMs), was previously

161 found to be significantly improved by using protocols that include cryo-fixation and freeze-
162 substitution (Knoops *et al.*, 2008; Snijder *et al.*, 2006). We now applied these advanced preservation
163 techniques, including newly developed protocols for high-pressure freezing (HPF), to MERS-CoV-
164 infected Vero cells. Images of similarly prepared SARS-CoV-infected Vero E6 cells are included for
165 comparison (Fig. 3f).

166 Compared to mock-infected control cells (Fig. 3e), different degrees of distinct alterations
167 were observed at 8 h p.i. Some cells contained relatively small DMV clusters (Fig. 3a,b; black
168 arrowheads, inset), whereas in others large numbers of DMVs occupied extensive areas of the
169 perinuclear region (Fig. 3c,d), differences that likely reflect different stages in infection progression.
170 The diameter of MERS-CoV-induced DMVs ranged from 150 to 320 nm, comparable to what was
171 previously measured for SARS-CoV-induced structures (Knoops *et al.*, 2008). An interesting
172 morphological difference with our previous studies of SARS-CoV-infected cells was the presence of a
173 dense inner DMV core, which can be attributed to technical differences in sample preparation. In
174 terms of ultrastructural preservation, HPF is widely considered superior to the previously used
175 plunge-freezing protocols. Also in the case of SARS-CoV (Fig. 3f) and the distantly related equine
176 arteritis virus (Knoops *et al.*, 2012), a similar dense DMV core became apparent when HPF was
177 employed. Although DMV cores are known to contain dsRNA, the implications of these
178 ultrastructural observations remain unclear. Interestingly, CMs were always surrounded by DMV
179 clusters and were only observed in cells that appeared to be more advanced in infection (Fig. 3c,d;
180 white arrows, inset). This observation strengthens the notion that DMV formation precedes the
181 development of CMs, as previously postulated for SARS-CoV (Knoops *et al.*, 2008).

182

183 **MERS-CoV-induced cytophatology and cell death.** In cell culture, many CoVs induce severe
184 cytopathic effect (CPE) and cell death. Infection with a number of CoVs can also induce extensive
185 syncytium formation, due to fusion activity of the viral spike protein at neutral pH (reviewed in
186 (Belouzard *et al.*, 2012). MERS-CoV-induced cytopathology was monitored by light microscopy
187 following low-m.o.i. inoculation of monkey and human cells (Fig. 4). In line with previous
188 observations (Zaki *et al.*, 2012), Vero cells developed clear CPE at 2 days post infection (d p.i.) and

189 detached at 3 d p.i. (Fig. 4a). Similar observations were made for Calu3/2B4 cells (Fig. 4b). In
190 contrast, MERS-CoV-infected Vero E6 cells displayed only mild CPE starting at 3 d p.i and cell death
191 was not complete after six days (Fig. 4c). The development of CPE in Huh7 cells was strikingly faster
192 compared to the three other cell lines and, following extensive syncytium formation, cells detached
193 already around 17 h (Fig. 4d). Given the low m.o.i. used and the viral replication kinetics (Fig. 1), the
194 syncytium formation in these only partially infected Huh7 cultures appeared to be a major factor in
195 CPE development. DPP4 expression on Vero and Huh7 cells (Raj *et al.*, 2013) and expression levels
196 of DPP4 on Calu3/2B4 and Vero E6 cells correlated with susceptibility to MERS-CoV (data not
197 shown).
198
199 **Development of an assay to screen for compounds inhibiting MERS-CoV replication.** The virus-
200 induced CPE in Vero and Huh7 cells was used to develop a first assay to screen for compounds that
201 inhibit MERS-CoV replication in cell culture. Vero cells were seeded in 96-well plates and infected at
202 an m.o.i. of 0.005 or 0.05 (Fig. 5a). After two and three days, CPE formation was monitored
203 microscopically and cytotoxicity was measured using a commercial cell viability assay. Moderate
204 CPE was observed on day 2, and by day 3 cell viability had dropped below 10% with both virus doses
205 used (Fig. 5a), indicating near-complete cell death. In MERS-CoV-infected Huh7 cells (Fig. 5b),
206 already after day 1, cell viability had dropped to 79% or 24% (after m.o.i. 0.005 or 0.05 infection,
207 respectively), which was in line with our observations on rapid syncytium formation and CPE in this
208 particular cell line (Fig. 4d). One day later, CPE was complete for both virus doses used and cells had
209 detached (Fig. 5b). Based on this comparison, further experiments were done using an m.o.i. of 0.005
210 and Huh7 and Vero cells were incubated for two or three days, respectively, before measuring cell
211 viability.
212 Previously, it was shown that replication of various CoVs, including SARS-CoV, can be
213 inhibited by the immunosuppressive drug CsA (de Wilde *et al.*, 2011; Pfefferle *et al.*, 2011).
214 Therefore, while testing whether the CPE-based assay described above could be used as an antiviral
215 screening method, we used CsA treatment to obtain a first proof of principle. Infected Vero cells were
216 given 3 or 9 μM of CsA and were analysed at 3 d p.i. At the concentrations used, CsA did not

217 adversely affect the viability of mock-infected cells (Fig. 5c). Treatment with 9 μM completely
218 inhibited CPE and left cell viability unchanged compared to mock-infected control cells. The
219 inhibitory effect of CsA was confirmed in Huh7 cells (Fig. 5d), which displayed reduced and lack of
220 CPE upon treatment with 7.5 μM and 15 μM CsA, respectively. These results were corroborated by
221 immunofluorescence microscopy analysis of CsA-treated and high m.o.i.-infected Vero and Huh7
222 cells and by determining virus titres released into the medium. Both assays confirmed an almost
223 complete block of MERS-CoV-infection (data not shown). However, as previously reported for other
224 CoVs (de Wilde *et al.*, 2011), a small fraction of MERS-CoV-infected cells appeared to be refractive
225 to CsA treatment and supported a low level of MERS-CoV replication, even at high CsA
226 concentrations (data not shown).
227
228 **Enhanced sensitivity of MERS-CoV to pegylated IFN-α treatment in comparison to SARS-CoV.**
229 Type I IFNs inhibit CoV replication and can protect against infection in animal models (Haagmans *et*
230 *al.*, 2004; Taguchi & Siddell, 1985). We therefore compared the effect of pegylated interferon-α
231 (PEG-IFN) treatment on MERS-CoV and SARS-CoV replication *in vitro*. Vero cells were given
232 PEG-IFN 4 h before low-m.o.i. infection, together with the inoculum or 4 h after infection. At 2 d p.i.
233 CPE was scored microscopically.
234 Treatment with PEG-IFN profoundly inhibited both MERS-CoV- and SARS-CoV-induced
235 CPE and RNA levels in a dose-dependent manner (Fig. 6). At 2 d p.i., SARS-CoV-induced CPE was
236 reduced for all time points of PEG-IFN addition when using a dose of at least 30 ng/ml PEG-IFN
237 (Fig. 6a), whereas MERS-CoV-induced CPE already decreased using a dose of 1 ng/ml (Fig. 6b). For
238 SARS-CoV, only pre-treatment with 1000 ng/ml PEG-IFN completely prevented CPE. For MERS-
239 CoV, complete inhibition of CPE was observed at much lower concentrations, specifically 3, 10 or 30
240 ng/ml when the drug was added to the cells before, during or after infection, respectively. Although
241 decreased CPE was also observed in SARS-CoV-infected cultures treated with 30 ng/ml PEG-IFN,
242 only a 30-fold reduction of viral RNA was detected in their medium at 2 d p.i. (Fig. 6c). For
243 comparison, treatment of MERS-CoV-infected cells with the same PEG-IFN dose completely blocked

244 CPE and reduced viral RNA levels in the medium 600- to 2,000-fold, depending on the timing of
245 PEG-IFN addition (Fig. 6d).

246 Our data revealed that in the same cell line MERS-CoV infection is 50-100 times more
247 sensitive to PEG-IFN treatment than SARS-CoV infection. This difference may be explained by
248 important lineage-specific genetic differences between these two zoonotic betacoronaviruses in terms
249 of accessory protein genes encoded in the 3' part of the genome (Snijder *et al.*, 2003; van Boheemen
250 *et al.*, 2012). In particular, MERS-CoV does not encode a homolog of the SARS-CoV ORF6 protein,
251 which was reported to block the IFN-induced nuclear translocation of phosphorylated transcription
252 factor STAT1. As nuclear translocation of p-STAT1 is essential for transcriptional activation of
253 downstream antiviral genes, the ORF6 protein makes SARS-CoV less sensitive to treatment with type
254 I IFN (Frieman *et al.*, 2007; Sims *et al.*, 2013). IFN-induced translocation of p-STAT1 was readily
255 observed in IFN-treated mock-infected Vero cells (Fig. 7a-d), but not in IFN-treated SARS-CoV-
256 infected cells (Fig. 7e,f). In contrast, in MERS-CoV-infected and IFN-treated cultures the
257 translocation of p-STAT1 was detected (Fig. 7g,h). Together with the data on IFN sensitivity (Fig. 5),
258 these observations highlight important differences between SARS-CoV and MERS-CoV in terms of
259 their interaction with the IFN signalling pathways.

260

261

262 **DISCUSSION**

263

264 Following the 2003 SARS epidemic, global CoV hunting efforts identified a wealth of previously
265 unknown family members, in particular in bat species from several continents (de Groot *et al.*, 2012).
266 Moreover, at least three of the four current 'established' human CoVs (NL63, 229E, and OC43) were
267 postulated to have originated from zoonotic reservoirs (Huynh *et al.*, 2012; Pfefferle *et al.*, 2009;
268 Vijgen *et al.*, 2005). Recently, about a decade after the SARS outbreak, MERS-CoV was identified as
269 the next zoonotic CoV (Zaki *et al.*, 2012) and appears to be highly pathogenic to humans: of the 49
270 cases confirmed thus far, 23 had a fatal outcome
271 (http://www.who.int/csr/don/archive/disease/coronavirus_infections/en/). Whether zoonotic CoVs
272 cause transient epidemics or establish a long-lasting relationship with the human host, an in-depth
273 understanding of virus-host interactions will be required to develop effective countermeasures. In this
274 study, we defined several basic but important parameters of MERS-CoV replication in cell culture
275 (Figs. 1-4). Among the tools for MERS-CoV research developed are immunoassays based on cross-
276 reacting antisera raised against other betacoronaviruses (Fig. 2) and a CPE-based assay that can be
277 used to screen for antiviral effects (Figs. 5-6).

278 Following the development of a high-throughput screening method for antiviral effects, proof
279 of principle was obtained using CsA, a recently discovered inhibitor of CoV replication (de Wilde *et*
280 *al.*, 2011; Pfefferle *et al.*, 2011). This drug affects the function of several members of the cellular
281 cyclophilin (Cyp) family and appears to block functional interactions between viral proteins and one
282 or multiple cyclophilin family members (Nagy *et al.*, 2011). Low-micromolar CsA concentrations
283 blocked MERS-CoV-induced CPE in Vero and Huh7 cells (9 μM and 15 μM, respectively) as
284 previously observed for other CoVs (de Wilde *et al.*, 2011; Pfefferle *et al.*, 2011). As in those
285 previous studies (de Wilde *et al.*, 2011), a small fraction of the cells somehow remained susceptible to
286 MERS-CoV infection, even at high CsA concentrations. Thus, virus replication could not be
287 completely eliminated, which may ultimately lead to the development of CsA resistance in cell
288 culture. In conclusion, these experiments established that monitoring MERS-CoV-induced CPE can

289 be a valuable and rapid tool in screening for the potential antiviral activity of e.g. small-molecule
290 compounds or FDA-approved drugs like PEG-IFN.

291 Type I IFN induction, a hallmark of the early innate immune response, is counteracted by
292 different CoV-encoded proteins. Despite these evasion strategies, IFN can be detected in sera of CoV-
293 infected mice and humans (Cameron *et al.*, 2012; Garlinghouse *et al.*, 1984; Taguchi & Siddell,
294 1985), and CoV-infected plasmacytoid DCs have been identified as a source of high IFN-α levels
295 (Cervantes-Barragan *et al.*, 2007; Roth-Cross *et al.*, 2007). The SARS-CoV ORF6 protein, however,
296 (partially) disrupts the downstream IFN-induced signalling in infected cells by inhibiting the nuclear
297 translocation of p-STAT1, a critical component of both the IFN-α and IFN-γ signalling pathways
298 (Frieman *et al.*, 2007). Although contributions from additional immune evasion mechanisms are
299 likely, the lack of a SARS-CoV ORF6 homolog (van Boheemen *et al.*, 2012) may be a major factor in
300 the higher sensitivity of MERS-CoV to PEG-IFN treatment, as observed in this study and other recent
301 work (Kindler *et al.*, 2013). This was further substantiated by the finding that nuclear translocation of
302 p-STAT1 is not blocked in MERS-CoV-infected cells (Fig. 7), which indicates that MERS-CoV has
303 not evolved an alternative strategy to achieve the same goal. MHV has been shown to be relatively
304 insensitive to IFN pre-treatment, however also this virus does not block activation and translocation of
305 p-STAT1 but instead inhibits the induction of a subset of ISGs by IFN-α/β (Rose *et al.*, 2010). Future
306 studies may elucidate whether MERS-CoV has evolved alternative strategies to cope with the host's
307 IFN response. In addition, it will be important to test whether MERS-CoV is attenuated *in vivo* as a
308 result of the relative high IFN sensitivity.

309 PEG-IFN is a registered drug used for the treatment of chronic hepatitis B and C infections in
310 humans (Bergman *et al.*, 2011). Several CoVs, including SARS-CoV, were shown to be sensitive to
311 both type I IFN treatment *in vitro* and PEG-IFN treatment *in vivo* (Haagmans *et al.*, 2004; Paragas *et*
312 *al.*, 2005; Zheng *et al.*, 2004), and in this study we established a relatively high sensitivity for MERS-
313 CoV. For example, in cynomolgus macaques plasma levels of 1-5 ng/ml were reached (Haagmans *et*
314 *al.*, 2004), a dose which in this study significantly reduced MERS-CoV replication *in vitro*. The
315 sensitivity of MERS-CoV to exogenous IFN suggests that administration of recombinant IFN merits

316 further evaluation as a therapeutic intervention strategy if new infections with the novel virus would
317 occur.
318
319 ## MATERIAL AND METHODS
320
321 **Cells culture and virus infection.** Vero cells (ATCC: CCL-81) were cultured in Eagle's minimal
322 essential medium (EMEM; Lonza) with 8% fetal calf serum (FCS; PAA) and antibiotics. Huh7 cells
323 were grown in Dulbecco's Modified Eagle Medium (DMEM; Lonza) containing 8% FCS, 2 mM L-
324 Glutamine (PAA), non-essential amino acids (PAA), and antibiotics. Vero E6 and Calu3/2B4 cells
325 were cultured as previously described (Snijder *et al.*, 2006; Yoshikawa *et al.*, 2010). Infection of
326 Vero, Vero E6, Huh7, and Calu3/2B4 cells with MERS-CoV (strain EMC/2012; (van Boheemen *et*
327 *al.*, 2012; Zaki *et al.*, 2012) at high multiplicity of infection (m.o.i. 5) was done in PBS containing 50
328 μg/ml DEAE-dextran and 2% FCS. Inoculations with a low dose (m.o.i. ≤ 0.05) of MERS-CoV or
329 SARS-CoV (strain HKU-39849; (Zeng *et al.*, 2003) were done directly in EMEM containing 2%
330 FCS. Virus titrations by plaque assay were performed as described before (van den Worm *et al.*,
331 2012). All work with live MERS-CoV and SARS-CoV was performed inside biosafety cabinets in
332 biosafety level 3 facilities at Leiden University Medical Center or Erasmus Medical Center.
333
334 **Antibodies and drugs.** Rabbit antisera recognizing the SARS-CoV replicase subunits nsp3, nsp4,
335 nsp5 and nsp8 have been described previously (Snijder *et al.*, 2006; van Hemert *et al.*, 2008b). Rabbit
336 antisera recognizing the SARS-CoV nucleocapsid (N) protein and MHV nsp4 were raised as
337 described (Snijder *et al.*, 1994). Antigens were a full-length recombinant SARS-CoV N protein
338 (purified from *E. coli*) and a synthetic peptide representing the 23 C-terminal residues of MHV nsp4,
339 respectively. p-STAT1 was detected with Alexa Fluor 488-labelled mouse-anti-STAT1 (pY701) (BD
340 Biosciences) and FITC-labelled anti-mouse-IgG was used to enhance the green fluorescence. Virus
341 infection was detected using the above-mentioned anti-nsp3 sera and Alexa Fluor 594-labeled anti-
342 rabbit IgG.

343 Cyclosporin A (CsA; Sigma) was dissolved in DMSO and a 10-mM stock was stored in aliquots for
344 single use at -20ºC. Peg-interferon alfa-2b (PEG-IFN; Pegintron, Merck, USA) was prepared
345 according to the manufacturer's instruction as a 100 µg/ml stock stored at 4ºC.
346
347 **Immunofluorescence microscopy.** Cells were grown on coverslips and fixed with 3%
348 paraformaldehyde in PBS or with 4% formaldehyde and 70% ethanol (p-STAT1 experiments),
349 permeabilized with 0.1% Triton X-100, and processed for immunofluorescence microscopy as
350 described previously (van der Meer *et al.*, 1998). Specimens were examined with a Zeiss Axioskop 2
351 fluorescence microscope with an Axiocam HRc camera and Zeiss Axiovision 4.4 software or with a
352 confocal microscope (Zeiss, LSM 700) (p-STAT1 experiments).
353
354 **Electron microscopy.** Vero cells were grown on sapphire discs and fixed at 8 h p.i. for 30 min at
355 room temperature with 3% paraformaldehyde and 0.25% glutaraldehyde in 0.1 M PHEM buffer pH
356 6.9 [60 mM piperazide-1,4-bis (2-ethanesulfonic acid), 25 mM HEPES, 2mM $MgCl_2$, 10mM EGTA]
357 containing 50% diluted Eagle's minimal essential medium and 1% FCS. Cells were stored in fixative
358 at 4°C for 72 h and then high-pressure frozen using a Leica EM PACT2. Freeze-substitution was
359 performed in an automated system (Leica AFS2) using as freeze-substitution medium acetone
360 containing 1% OsO_4, 0.5% uranyl acetate and 10% H_2O. First, the samples were maintained at -90°C
361 for 6 h in this medium and then slowly warmed to -20°C within 14 h, kept at -20°C for 1 h, warmed to
362 0°C at a 5°C/h rate and left at 0°C for 1 h before letting the samples reach room temperature. After
363 washing with acetone, the samples were gradually infiltrated with epoxy resin LX-112 and
364 polymerized at 60°C. The samples were cut into thin sections (100 nm) and counterstained with
365 uranyl acetate and lead citrate. Imaging was performed in an FEI Tecnai12 TWIN electron
366 microscope operating at 120 kV and equipped with an Eagle 4k cooled slow-scan charge-coupled
367 device (CCD) camera (FEI company). The images were acquired using binning mode 2.
368
369 **Intracellular viral RNA analysis.** Isolation of intracellular viral RNA was described previously (van
370 Kasteren *et al.*, 2013). After drying of the gel, viral mRNAs were detected by hybridization with a

371 ^{32}P-labeled oligonucleotide probe (5'-GCAAATCATCTAATTAGCCTAATC-3') complementary to
372 the 3'end of all MERS-CoV mRNAs. Equal loading was verified in a second hybridization using a
373 ^{32}P-labeled oligonucleotide probe (5'-GTAACCCGTTGAACCCCATT-3') recognizing 18S
374 ribosomal RNA (van Hemert *et al.*, 2008a). ImageQuant TL (GE Healthcare) software was used for
375 quantification.
376
377 **Real-time reverse transcription-polymerase chain reaction (RT-PCR).** RNA from 200 µl culture
378 medium of CoV-infected cells was isolated with the MagnaPure LC total nucleic acid isolation kit
379 (Roche) and eluted in 100 µl. RT-PCR conditions for quantifying MERS-CoV and SARS-CoV RNA
380 and amplification parameters were described previously (Kuiken *et al.*, 2003; Raj *et al.*, 2013).
381 Dilutions of viral RNA isolated from MERS-CoV or SARS-CoV virus stocks with a known virus titre
382 were used to produce a standard curve.
383
384 **Development of a screening assay for antiviral compounds.** Huh7 or Vero cells were seeded in 96-
385 well plates at a density of 10^4 or $2x10^4$ cells per well, respectively. After overnight growth, cells were
386 infected with an m.o.i. of 0.005 or 0.05. One to three days after incubation, differences in cell viability
387 caused by virus-induced CPE or by compound-specific side effects were analysed using the CellTiter
388 96® AQ_{ueous} Non-Radioactive Cell Proliferation Assay (Promega), according to the manufacturer's
389 instructions. Absorbance (A_{490}) was measured using a Berthold Mithras LB 940 96-well plate reader.
390 Infected cells were given CsA or DMSO (solvent control) prior to infection (m.o.i 0.005). Cytotoxic
391 effects caused by CsA treatment alone were monitored in parallel plates containing mock-infected
392 cells.
393
394 **IFN sensitivity and p-STAT1 translocation experiments.** One day prior to infection, Vero cells
395 were plated at a density of 10^4 cells per well in a 96-well plate format. At -4, 0 and 4 h p.i., cells were
396 incubated with 0 to 1000 ng/ml PEG-IFN in 250 µl. At t=0 h, all wells were washed with PBS and
397 infected with MERS-CoV or SARS-CoV (100 $TCID_{50}$ per 100 µl medium). Those cultures receiving
398 treatment from t=-4 or t=0 were infected in the presence of the indicated concentration PEG-IFN.

399 After 1 h, 150 µl medium was added to the cultures of t=-4 or t=0 cultures, and 100 µl medium was
400 added to the untreated cultures, which at 4 h p.i. received 50 µl medium supplemented with PEG-IFN
401 to reach a final concentration of 0 to 1000 ng/ml PEG-IFN. At 48 h p.i., RNA was isolated from 50 µl
402 cell culture supernatant and quantified using virus-specific real time RT-PCR assays (see above).
403 Furthermore at 48 h p.i., CPE was scored microscopically as either (0) none, (1) mild, (2) moderate,
404 (3) severe or (4) complete.

405 For p-STAT1 nuclear translocation experiments, Vero cells were infected with MERS-CoV
406 or SARS-CoV (m.o.i. 1). At 8 h p.i., cells were treated with 1000 ng/ml PEG-IFN for 30 min and
407 fixed with 4% formaldehyde and 70% ethanol and subsequently stained for presence of viral antigen
408 and p-STAT1 translocation.

409

410

ACKNOWLEDGEMENTS

We are grateful to Ron Fouchier, Chris Lauber and Alexander Gorbalenya for helpful discussions, and we thank Dennis Ninaber and Corrine Beugeling for technical assistance. This research was supported in part by TOP grant 700.57.301 from the Council for Chemical Sciences (CW) and MEERVOUD grant 836.10.003 from the Council for Earth and Life Sciences (ALW) of the Netherlands Organization for Scientific Research (NWO) and the EU-FP7-Health project SILVER (Grant #260644).

420 **FIGURE LEGENDS**

421

422 **Fig 1. Kinetics of MERS-CoV replication in Vero and Huh7 cells.** Vero and Huh7 cells were
423 infected with MERS-CoV (m.o.i. 5). (a) Hybridization analysis of viral mRNAs isolated from MERS-
424 CoV-infected cells using an oligonucleotide recognizing the viral genome and all sg mRNAs.
425 Additional minor bands of ~3 and ~4 kb were observed (*) and may represent additional viral mRNA
426 species that remain to be studied in more detail. However, the corresponding positions in the ORF4a/b
427 and ORF5 coding regions do not contain a canonical core TRS sequence (AACGAA; (van Boheemen
428 *et al.*, 2012) that might provide a direct explanation for their synthesis. (b) Analysis of the relative
429 molarities of viral genome and each of the sg mRNAs (% of total viral mRNA). mRNA sizes were
430 calculated on the basis of the TRS positions in the viral genome sequence (van Boheemen *et al.*,
431 2012). Phosphorimager quantification was performed on the gel lanes with the RNA samples isolated
432 from Vero cells at 10, 13 and 24 h p.i. (Fig. 1a; lanes 3, 4, and 5; avg ± SD). (c) Release of infectious
433 MERS-CoV progeny into the medium of infected Vero or Huh7 cells at the indicated time points, as
434 determined by plaque assay (avg ± SD; n=4).

435

436 **Fig 2. Selected rabbit antisera raised against SARS-CoV and MHV nsps cross-react with**
437 **MERS-CoV proteins.** (a) MERS-CoV-infected Vero cells (m.o.i. 5) were fixed at 8 h p.i. For
438 immunofluorescence microscopy, cells were double-labelled with a mouse monoclonal antibody
439 recognizing dsRNA (bottom row) and rabbit antisera raised against SARS-CoV nsp3, nsp4, nsp5 or
440 nsp8, or MHV nsp4 (top row). Bar, 20 µm. (b) Sequence comparison of the C-terminal domain of
441 nsp4 of SARS-CoV (isolate Frankfurt 1), MERS-CoV (strain EMC/2012) and MHV (strain A59). The
442 SARS-CoV and MHV sequences corresponds to the synthetic peptides used to raise rabbit anti-nsp4
443 sera. Residues conserved in all three viruses are highlighted in yellow, whereas residues conserved in
444 two out of three are highlighted in grey. Amino acid numbers refer to the full-length pp1a sequence.
445 (c) Monolayers of Vero, Vero E6, Huh7 and Calu3/2B4 cells were infected with MERS-CoV (m.o.i.
446 5) and double-labelled for dsRNA (green) and nsp3 (red). Bar, 40 µm.

447

448 **Fig.3. Membrane structures induced by MERS-CoV infection.** Electron micrographs of thin
449 sections (100 nm) of (a-d) MERS-CoV-infected Vero cells at 8 h p.i. (a) Low magnification images of
450 a cell containing a small cluster of double-membrane vesicles, enlarged in (b). Some DMVs are
451 indicated by black arrowheads and the inset displays a close-up of the boxed DMV in (b). (c)
452 Extensive membrane alterations in the perinuclear region. The boxed area in (c) is displayed at higher
453 magnification in (d), where CMs (white arrows, inset) embedded in clusters of DMVs (black
454 arrowheads) can be observed. For comparison, (e) shows the unaltered cytoplasm of a mock-infected
455 cell and (f) contains SARS-CoV-induced DMV (black arrowheads) as observed after HPF and freeze
456 substitution. N, nucleus; m, mitochondria. Scale bars, 2 µm (a,c,e), 500 nm (b,d,f).

457

458 **Fig 4. MERS-CoV infection induces severe cytopathology in monkey and human cell lines.**
459 **Monolayers of Vero (a), Calu3/2B4 (b), Vero E6 (c)** and Huh7 (d) cells infected with MERS-CoV
460 (m.o.i. 0.05) and analysed by light microscope at the indicated time points. Bar, 100 µm.

461

462 **Fig. 5. Development of an assay to screen for compounds inhibiting MERS-CoV replication.**
463 (a,c) Vero and (b,d) Huh7 cells in a 96-well plate format were infected at an m.o.i. of 0.005 or 0.05.
464 Mock-infected cells were used as reference for unchanged cell viability (their relative viability was set
465 at 100%). (a) Infected Vero cells were incubated for 2 or 3 days and (b) Huh7 cells were incubated for
466 1 or 2 days. (c) Vero cells were infected with MERS-CoV (m.o.i. 0.005) in the presence of 3 µM or 9
467 µM CsA, or 0.09% DMSO as solvent control. (d) Huh7 cells were infected with MERS-CoV (m.o.i.
468 0.005) in the presence of 3.75 to 15 µM CsA, or 0.15% DMSO. (c,d) Graphs show the results of a
469 representative experiment (avg ± SD; n=4). All experiments were repeated at least twice.

470

471 **Fig. 6. Sensitivity of MERS-CoV and SARS-CoV to PEG-IFN.** Vero cells were incubated with 0 to
472 1000 ng/ml PEG-IFN at t=-4, t=0, at t=4 h p.i. Cells were infected with 100 $TCID_{50}$ virus per well.
473 (a,b) At 2 d p.i. cells were examined for CPE. Effect of PEG-IFN treatment on CPE induced by (a)

474 SARS-CoV or (b) MERS-CoV. CPE was scored as either (0) none, (1) mild, (2) moderate, (3) severe
475 or (4) complete. (c,d) Viral genomes in the culture medium of virus-infected cells were determined by
476 RT-PCR. Influence of PEG-IFN treatment on the viral RNA load (genome equivalents (gen. eq.) per
477 ml) in the supernatants of cells infected with (c) SARS-CoV or (d) MERS-CoV.
478
479 **Fig. 7. IFN–α induced nuclear translocation of p-STAT1 in MERS-CoV-infected Vero cells.**
480 Confocal immunofluorescence microscopy of uninfected Vero cells (a-d) and Vero cells infected
481 (m.o.i. 1) with SARS-CoV (e,f) or MERS-CoV (g,h). At 8 h p.i. cells were (a, b) left untreated or (c-
482 h) treated with 1000 ng/ml PEG-IFN for 30 minutes, fixed and double-labelled with antisera against
483 SARS-CoV nsp3 (red; a-h), or p-STAT1 (green; b,d,f,h), and nuclear DNA was stained with DAPI
484 (blue; a,c,e,g).
485

486 **REFERENCES**

487

488 **Belouzard, S., Millet, J. K., Licitra, B. N. & Whittaker, G. R. (2012).** Mechanisms of coronavirus
489 cell entry mediated by the viral spike protein. *Viruses* **4**, 1011-1033.

490 **Bergman, S. J., Ferguson, M. C. & Santanello, C. (2011).** Interferons as therapeutic agents for
491 infectious diseases. *Infect Dis Clin North Am* **25**, 819-834.

492 **Brockway, S. M., Clay, C. T., Lu, X. T. & Denison, M. R. (2003).** Characterization of the
493 expression, intracellular localization, and replication complex association of the putative mouse
494 hepatitis virus RNA-dependent RNA polymerase. *J Virol* **77**, 10515-10527.

495 **Cameron, M. J., Kelvin, A. A., Leon, A. J., Cameron, C. M., Ran, L., Xu, L., Chu, Y. K.,**
496 **Danesh, A., Fang, Y. & other authors (2012).** Lack of innate interferon responses during SARS
497 coronavirus infection in a vaccination and reinfection ferret model. *PLoS One* **7**, e45842.

498 **Cervantes-Barragan, L., Zust, R., Weber, F., Spiegel, M., Lang, K. S., Akira, S., Thiel, V. &**
499 **Ludewig, B. (2007).** Control of coronavirus infection through plasmacytoid dendritic-cell-derived
500 type I interferon. *Blood* **109**, 1131-1137.

501 **de Groot, R. J., Cowley, J. A., Enjuanes, L., Faaberg, K. S., Perlman, S., Rottier, P. J., Snijder,**
502 **E. J., Ziebuhr, J. & Gorbalenya, A. E. (2012).** Order of Nidovirales. In *Virus Taxonomy, the 9th*
503 *Report of the International Committee on Taxonomy of Viruses*, pp. 785-795. Edited by A. King, M.
504 Adams, E. Carstens & E. J. Lefkowitz: Academic Press.

505 **de Groot, R. J., Baker, S. C., Baric, R. S., Brown, C. S., Drosten, C., Enjuanes, L., Fouchier, R.**
506 **A., Galiano, M., Gorbalenya, A. E. & other authors (2013).** Middle East Respiratory Syndrome
507 Coronavirus (MERS-CoV); Announcement of the Coronavirus Study Group. *J Virol* **87**, in press
508 (doi:10.1128/JVI.01244-13).

509 **de Wilde, A. H., Zevenhoven-Dobbe, J. C., van der Meer, Y., Thiel, V., Narayanan, K., Makino,**
510 **S., Snijder, E. J. & van Hemert, M. J. (2011).** Cyclosporin A inhibits the replication of diverse
511 coronaviruses. *J Gen Virol* **92**, 2542-2548.

512 **Drosten, C., Gunther, S., Preiser, W., van der Werf, S., Brodt, H. R., Becker, S., Rabenau, H.,**
513 **Panning, M., Kolesnikova, L. & other authors (2003).** Identification of a novel coronavirus in
514 patients with severe acute respiratory syndrome. *N Engl J Med* **348**, 1967-1976.
515 **Fouchier, R. A., Hartwig, N. G., Bestebroer, T. M., Niemeyer, B., de Jong, J. C., Simon, J. H. &**
516 **Osterhaus, A. D. (2004).** A previously undescribed coronavirus associated with respiratory disease in
517 humans. *Proc Natl Acad Sci USA* **101**, 6212-6216.
518 **Frieman, M., Yount, B., Heise, M., Kopecky-Bromberg, S. A., Palese, P. & Baric, R. S. (2007).**
519 Severe acute respiratory syndrome coronavirus ORF6 antagonizes STAT1 function by sequestering
520 nuclear import factors on the rough endoplasmic reticulum/Golgi membrane. *J Virol* **81**, 9812-9824.
521 **Garlinghouse, L. E., Jr., Smith, A. L. & Holford, T. (1984).** The biological relationship of mouse
522 hepatitis virus (MHV) strains and interferon: in vitro induction and sensitivities. *Arch Virol* **82**, 19-29.
523 **Gorbalenya, A. E., Enjuanes, L., Ziebuhr, J. & Snijder, E. J. (2006).** Nidovirales: evolving the
524 largest RNA virus genome. *Virus Res* **117**, 17-37.
525 **Gosert, R., Kanjanahaluethai, A., Egger, D., Bienz, K. & Baker, S. C. (2002).** RNA replication of
526 mouse hepatitis virus takes place at double-membrane vesicles. *J Virol* **76**, 3697-3708.
527 **Haagmans, B. L., Kuiken, T., Martina, B. E., Fouchier, R. A., Rimmelzwaan, G. F., van**
528 **Amerongen, G., van Riel, D., de Jong, T., Itamura, S. & other authors (2004).** Pegylated
529 interferon-alpha protects type 1 pneumocytes against SARS coronavirus infection in macaques. *Nat*
530 *Med* **10**, 290-293.
531 **Hamre, D. & Procknow, J. J. (1966).** A new virus isolated from the human respiratory tract. *Proc*
532 *Soc Exp Biol Med* **121**, 190-193.
533 **Hussain, S., Perlman, S. & Gallagher, T. M. (2008).** Severe acute respiratory syndrome coronavirus
534 protein 6 accelerates murine hepatitis virus infections by more than one mechanism. *J Virol* **82**, 7212-
535 7222.
536 **Huynh, J., Li, S., Yount, B., Smith, A., Sturges, L., Olsen, J. C., Nagel, J., Johnson, J. B.,**
537 **Agnihothram, S. & other authors (2012).** Evidence supporting a zoonotic origin of human
538 coronavirus strain NL63. *J Virol* **86**, 12816-12825.

539 **Kindler, E., Jonsdottir, H. R., Muth, D., Hamming, O. J., Hartmann, R., Rodriguez, R., Geffers,**
540 **R., Fouchier, R. A., Drosten, C. & other authors (2013).** Efficient Replication of the Novel Human
541 Betacoronavirus EMC on Primary Human Epithelium Highlights Its Zoonotic Potential. *MBio* **4**,
542 e00611-00612.
543 **Knoops, K., Barcena, M., Limpens, R. W., Koster, A. J., Mommaas, A. M. & Snijder, E. J.**
544 **(2012).** Ultrastructural characterization of arterivirus replication structures: reshaping the endoplasmic
545 reticulum to accommodate viral RNA synthesis. *J Virol* **86**, 2474-2487.
546 **Knoops, K., Kikkert, M., Worm, S. H., Zevenhoven-Dobbe, J. C., van der Meer, Y., Koster, A.**
547 **J., Mommaas, A. M. & Snijder, E. J. (2008).** SARS-coronavirus replication is supported by a
548 reticulovesicular network of modified endoplasmic reticulum. *PLoS Biol* **6**, e226.
549 **Kopecky-Bromberg, S. A., Martinez-Sobrido, L. & Palese, P. (2006).** 7a protein of severe acute
550 respiratory syndrome coronavirus inhibits cellular protein synthesis and activates p38 mitogen-
551 activated protein kinase. *J Virol* **80**, 785-793.
552 **Ksiazek, T. G., Erdman, D., Goldsmith, C. S., Zaki, S. R., Peret, T., Emery, S., Tong, S., Urbani,**
553 **C., Comer, J. A. & other authors (2003).** A novel coronavirus associated with severe acute
554 respiratory syndrome. *N Engl J Med* **348**, 1953-1966.
555 **Kuiken, T., Fouchier, R. A., Schutten, M., Rimmelzwaan, G. F., van Amerongen, G., van Riel,**
556 **D., Laman, J. D., de Jong, T., van Doornum, G. & other authors (2003).** Newly discovered
557 coronavirus as the primary cause of severe acute respiratory syndrome. *Lancet* **362**, 263-270.
558 **Lau, S. K., Woo, P. C., Li, K. S., Huang, Y., Tsoi, H. W., Wong, B. H., Wong, S. S., Leung, S. Y.,**
559 **Chan, K. H. & other authors (2005).** Severe acute respiratory syndrome coronavirus-like virus in
560 Chinese horseshoe bats. *Proc Natl Acad Sci USA* **102**, 14040-14045.
561 **Li, W., Shi, Z., Yu, M., Ren, W., Smith, C., Epstein, J. H., Wang, H., Crameri, G., Hu, Z. &**
562 **other authors (2005).** Bats are natural reservoirs of SARS-like coronaviruses. *Science* **310**, 676-679.
563 **McIntosh, K., Dees, J. H., Becker, W. B., Kapikian, A. Z. & Chanock, R. M. (1967).** Recovery in
564 tracheal organ cultures of novel viruses from patients with respiratory disease. *Proc Natl Acad Sci*
565 *USA* **57**, 933-940.

566 **Muller, M. A., Raj, V. S., Muth, D., Meyer, B., Kallies, S., Smits, S. L., Wollny, R., Bestebroer,**
567 **T. M., Specht, S. & other authors (2012).** Human Coronavirus EMC Does Not Require the SARS-
568 Coronavirus Receptor and Maintains Broad Replicative Capability in Mammalian Cell Lines. *MBio* **3**,
569 e00515-00512.

570 **Nagy, P. D., Wang, R. Y., Pogany, J., Hafren, A. & Makinen, K. (2011).** Emerging picture of host
571 chaperone and cyclophilin roles in RNA virus replication. *Virology* **411**, 374-382.

572 **Paragas, J., Blatt, L. M., Hartmann, C., Huggins, J. W. & Endy, T. P. (2005).** Interferon alfacon1
573 is an inhibitor of SARS-corona virus in cell-based models. *Antiviral Res* **66**, 99-102.

574 **Perlman, S. & Netland, J. (2009).** Coronaviruses post-SARS: update on replication and
575 pathogenesis. *Nat Rev Microbiol* **7**, 439-450.

576 **Pfefferle, S., Oppong, S., Drexler, J. F., Gloza-Rausch, F., Ipsen, A., Seebens, A., Muller, M. A.,**
577 **Annan, A., Vallo, P. & other authors (2009).** Distant relatives of severe acute respiratory syndrome
578 coronavirus and close relatives of human coronavirus 229E in bats, Ghana. *Emerg Infect Dis* **15**,
579 1377-1384.

580 **Pfefferle, S., Schopf, J., Kogl, M., Friedel, C. C., Muller, M. A., Carbajo-Lozoya, J., Stellberger,**
581 **T., von Dall'armi, E., Herzog, P. & other authors (2011).** The SARS-Coronavirus-Host
582 Interactome: Identification of Cyclophilins as Target for Pan-Coronavirus Inhibitors. *PLoS Pathog* **7**,
583 e1002331.

584 **Raj, V. S., Mou, H., Smits, S. L., Dekkers, D. H., Muller, M. A., Dijkman, R., Muth, D.,**
585 **Demmers, J. A., Zaki, A. & other authors (2013).** Dipeptidyl peptidase 4 is a functional receptor for
586 the emerging human coronavirus-EMC. *Nature* **495**, 251-254.

587 **Randall, R. E. & Goodbourn, S. (2008).** Interferons and viruses: an interplay between induction,
588 signalling, antiviral responses and virus countermeasures. *J Gen Virol* **89**, 1-47.

589 **Ratia, K., Saikatendu, K. S., Santarsiero, B. D., Barretto, N., Baker, S. C., Stevens, R. C. &**
590 **Mesecar, A. D. (2006).** Severe acute respiratory syndrome coronavirus papain-like protease: structure
591 of a viral deubiquitinating enzyme. *Proc Natl Acad Sci USA* **103**, 5717-5722.

592 **Rose, K. M., Elliott, R., Martinez-Sobrido, L., Garcia-Sastre, A. & Weiss, S. R. (2010).** Murine
593 coronavirus delays expression of a subset of interferon-stimulated genes. *J Virol* **84**, 5656-5669.

594 **Roth-Cross, J. K., Martinez-Sobrido, L., Scott, E. P., Garcia-Sastre, A. & Weiss, S. R. (2007).**
595 Inhibition of the alpha/beta interferon response by mouse hepatitis virus at multiple levels. *J Virol* **81**,
596 7189-7199.
597 **Sims, A. C., Tilton, S. C., Menachery, V. D., Gralinski, L. E., Schafer, A., Matzke, M. M.,**
598 **Webb-Robertson, B. J., Chang, J., Luna, M. L. & other authors (2013).** Release of severe acute
599 respiratory syndrome coronavirus nuclear import block enhances host transcription in human lung
600 cells. *J Virol* **87**, 3885-3902.
601 **Snijder, E. J., Wassenaar, A. L. & Spaan, W. J. (1994).** Proteolytic processing of the replicase
602 ORF1a protein of equine arteritis virus. *J Virol* **68**, 5755-5764.
603 **Snijder, E. J., van der, M. Y., Zevenhoven-Dobbe, J., Onderwater, J. J., van der, M. J., Koerten,**
604 **H. K. & Mommaas, A. M. (2006).** Ultrastructure and origin of membrane vesicles associated with
605 the severe acute respiratory syndrome coronavirus replication complex. *J Virol* **80**, 5927-5940.
606 **Snijder, E. J., Bredenbeek, P. J., Dobbe, J. C., Thiel, V., Ziebuhr, J., Poon, L. L., Guan, Y.,**
607 **Rozanov, M., Spaan, W. J. & other authors (2003).** Unique and conserved features of genome and
608 proteome of SARS-coronavirus, an early split-off from the coronavirus group 2 lineage. *J Mol Biol*
609 **331**, 991-1004.
610 **Stertz, S., Reichelt, M., Spiegel, M., Kuri, T., Martinez-Sobrido, L., Garcia-Sastre, A., Weber, F.**
611 **& Kochs, G. (2007).** The intracellular sites of early replication and budding of SARS-coronavirus.
612 *Virology* **361**, 304-315.
613 **Taguchi, F. & Siddell, S. G. (1985).** Difference in sensitivity to interferon among mouse hepatitis
614 viruses with high and low virulence for mice. *Virology* **147**, 41-48.
615 **Ulasli, M., Verheije, M. H., de Haan, C. A. & Reggiori, F. (2010).** Qualitative and quantitative
616 ultrastructural analysis of the membrane rearrangements induced by coronavirus. *Cell Microbiol* **12**,
617 844-861.
618 **van Boheemen, S., de Graaf, M., Lauber, C., Bestebroer, T. M., Raj, V. S., Zaki, A. M.,**
619 **Osterhaus, A. D., Haagmans, B. L., Gorbalenya, A. E. & other authors (2012).** Genomic
620 characterization of a newly discovered coronavirus associated with acute respiratory distress
621 syndrome in humans. *MBio* **3**, e00473-00412.

622 **van den Worm, S. H., Eriksson, K. K., Zevenhoven, J. C., Weber, F., Zust, R., Kuri, T.,**
623 **Dijkman, R., Chang, G., Siddell, S. G. & other authors (2012).** Reverse genetics of SARS-related
624 coronavirus using vaccinia virus-based recombination. *PLoS One* **7**, e32857.
625 **van der Hoek, L., Pyrc, K., Jebbink, M. F., Vermeulen-Oost, W., Berkhout, R. J., Wolthers, K.**
626 **C., Wertheim-van Dillen, P. M., Kaandorp, J., Spaargaren, J. & other authors (2004).**
627 Identification of a new human coronavirus. *Nat Med* **10**, 368-373.
628 **van der Meer, Y., van Tol, H., Krijnse Locker, J. & Snijder, E. J. (1998).** ORF1a-encoded
629 replicase subunits are involved in the membrane association of the arterivirus replication complex. *J*
630 *Virol* **72**, 6689-6698.
631 **van Hemert, M. J., de Wilde, A. H., Gorbalenya, A. E. & Snijder, E. J. (2008a).** The in vitro RNA
632 synthesizing activity of the isolated arterivirus replication/transcription complex is dependent on a
633 host factor. *J Biol Chem* **283**, 16525-16536.
634 **van Hemert, M. J., van den Worm, S. H., Knoops, K., Mommaas, A. M., Gorbalenya, A. E. &**
635 **Snijder, E. J. (2008b).** SARS-coronavirus replication/transcription complexes are membrane-
636 protected and need a host factor for activity in vitro. *PLoS Pathog* **4**, e1000054.
637 **van Kasteren, P. B., Bailey-Elkin, B. A., James, T. W., Ninaber, D. K., Beugeling, C.,**
638 **Khajehpour, M., Snijder, E. J., Mark, B. L. & Kikkert, M. (2013).** Deubiquitinase function of
639 arterivirus papain-like protease 2 suppresses the innate immune response in infected host cells. *Proc*
640 *Natl Acad Sci USA* **110**, E838-847.
641 **Versteeg, G. A., Bredenbeek, P. J., van den Worm, S. H. & Spaan, W. J. (2007).** Group 2
642 coronaviruses prevent immediate early interferon induction by protection of viral RNA from host cell
643 recognition. *Virology* **361**, 18-26.
644 **Vijaykrishna, D., Smith, G. J., Zhang, J. X., Peiris, J. S., Chen, H. & Guan, Y. (2007).**
645 Evolutionary insights into the ecology of coronaviruses. *J Virol* **81**, 4012-4020.
646 **Vijgen, L., Keyaerts, E., Moes, E., Thoelen, I., Wollants, E., Lemey, P., Vandamme, A. M. &**
647 **Van Ranst, M. (2005).** Complete genomic sequence of human coronavirus OC43: molecular clock
648 analysis suggests a relatively recent zoonotic coronavirus transmission event. *J Virol* **79**, 1595-1604.

649 **Weber, F., Wagner, V., Rasmussen, S. B., Hartmann, R. & Paludan, S. R. (2006).** Double-
650 stranded RNA is produced by positive-strand RNA viruses and DNA viruses but not in detectable
651 amounts by negative-strand RNA viruses. *J Virol* **80**, 5059-5064.

652 **Woo, P. C., Lau, S. K., Chu, C. M., Chan, K. H., Tsoi, H. W., Huang, Y., Wong, B. H., Poon, R.**
653 **W., Cai, J. J. & other authors (2005).** Characterization and complete genome sequence of a novel
654 coronavirus, coronavirus HKU1, from patients with pneumonia. *J Virol* **79**, 884-895.

655 **Woo, P. C., Wang, M., Lau, S. K., Xu, H., Poon, R. W., Guo, R., Wong, B. H., Gao, K., Tsoi, H.**
656 **W. & other authors (2007).** Comparative analysis of twelve genomes of three novel group 2c and
657 group 2d coronaviruses reveals unique group and subgroup features. *J Virol* **81**, 1574-1585.

658 **Yoshikawa, T., Hill, T. E., Yoshikawa, N., Popov, V. L., Galindo, C. L., Garner, H. R., Peters, C.**
659 **J. & Tseng, C. T. (2010).** Dynamic innate immune responses of human bronchial epithelial cells to
660 severe acute respiratory syndrome-associated coronavirus infection. *PLoS One* **5**, e8729.

661 **Zaki, A. M., van Boheemen, S., Bestebroer, T. M., Osterhaus, A. D. & Fouchier, R. A. (2012).**
662 Isolation of a novel coronavirus from a man with pneumonia in Saudi Arabia. *N Engl J Med* **367**,
663 1814-1820.

664 **Zeng, F. Y., Chan, C. W., Chan, M. N., Chen, J. D., Chow, K. Y., Hon, C. C., Hui, K. H., Li, J.,**
665 **Li, V. Y. & other authors (2003).** The complete genome sequence of severe acute respiratory
666 syndrome coronavirus strain HKU-39849 (HK-39). *Exp Biol Med* **228**, 866-873.

667 **Zheng, B., He, M. L., Wong, K. L., Lum, C. T., Poon, L. L., Peng, Y., Guan, Y., Lin, M. C. &**
668 **Kung, H. F. (2004).** Potent inhibition of SARS-associated coronavirus (SCOV) infection and
669 replication by type I interferons (IFN-alpha/beta) but not by type II interferon (IFN-gamma). *J*
670 *Interferon Cytokine Res* **24**, 388-390.

671 **Zhong, Y., Tan, Y. W. & Liu, D. X. (2012).** Recent progress in studies of arterivirus- and
672 coronavirus-host interactions. *Viruses* **4**, 980-1010.

673 **Zhou, P., Li, H., Wang, H., Wang, L. F. & Shi, Z. (2012).** Bat severe acute respiratory syndrome-
674 like coronavirus ORF3b homologues display different interferon antagonist activities. *J Gen Virol* **93**,
675 275-281.

676 **Zust, R., Cervantes-Barragan, L., Habjan, M., Maier, R., Neuman, B. W., Ziebuhr, J., Szretter,**
677 **K. J., Baker, S. C., Barchet, W. & other authors (2011).** Ribose 2'-O-methylation provides a
678 molecular signature for the distinction of self and non-self mRNA dependent on the RNA sensor
679 Mda5. *Nat Immunol* **12**, 137-143.
680
681

a

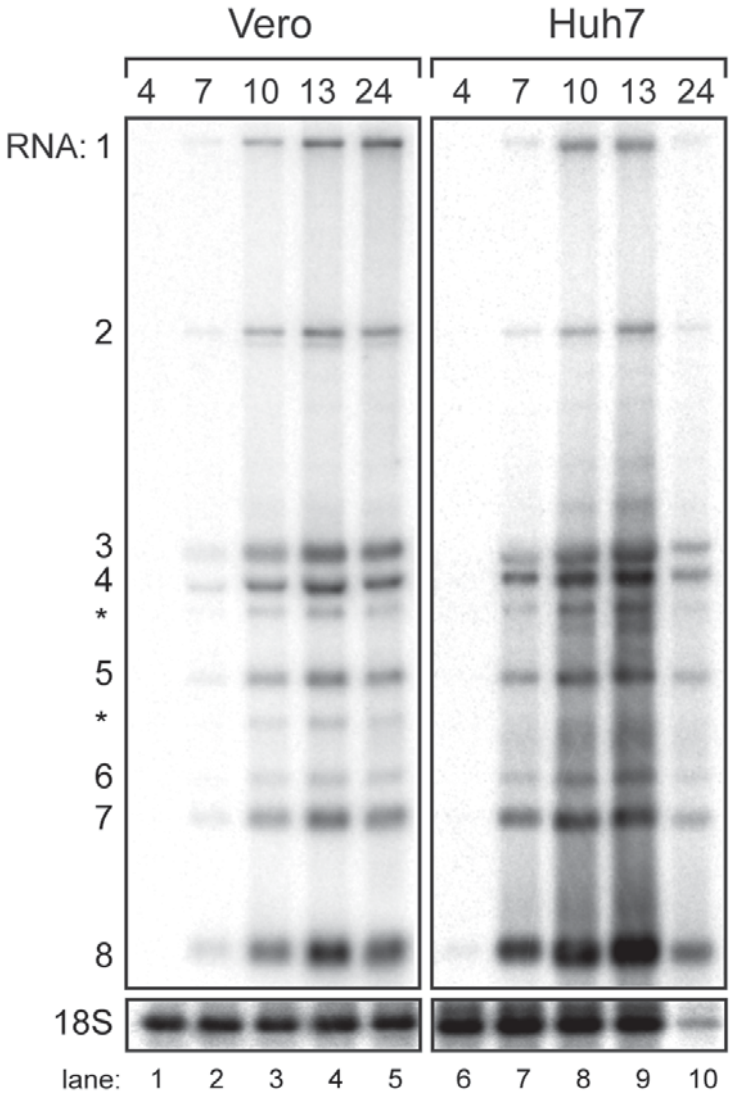

b

RNA	size (kb)	abundance (%)*
1	30.1	4.1 ± 1.1
2	8.8	4.5 ± 0.9
3	4.7	12.5 ± 1.4
4	4.3	12.1 ± 0.1
5	3.4	6.7 ± 0.6
6	2.6	1.4 ± 0.5
7	2.3	12.3 ± 3.1
8	1.7	43.6 ± 3.3

c

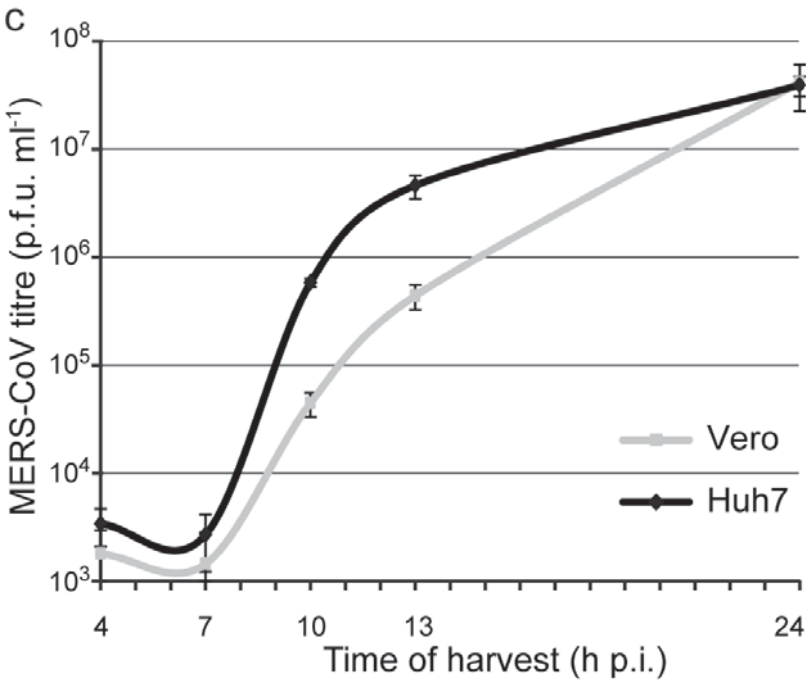

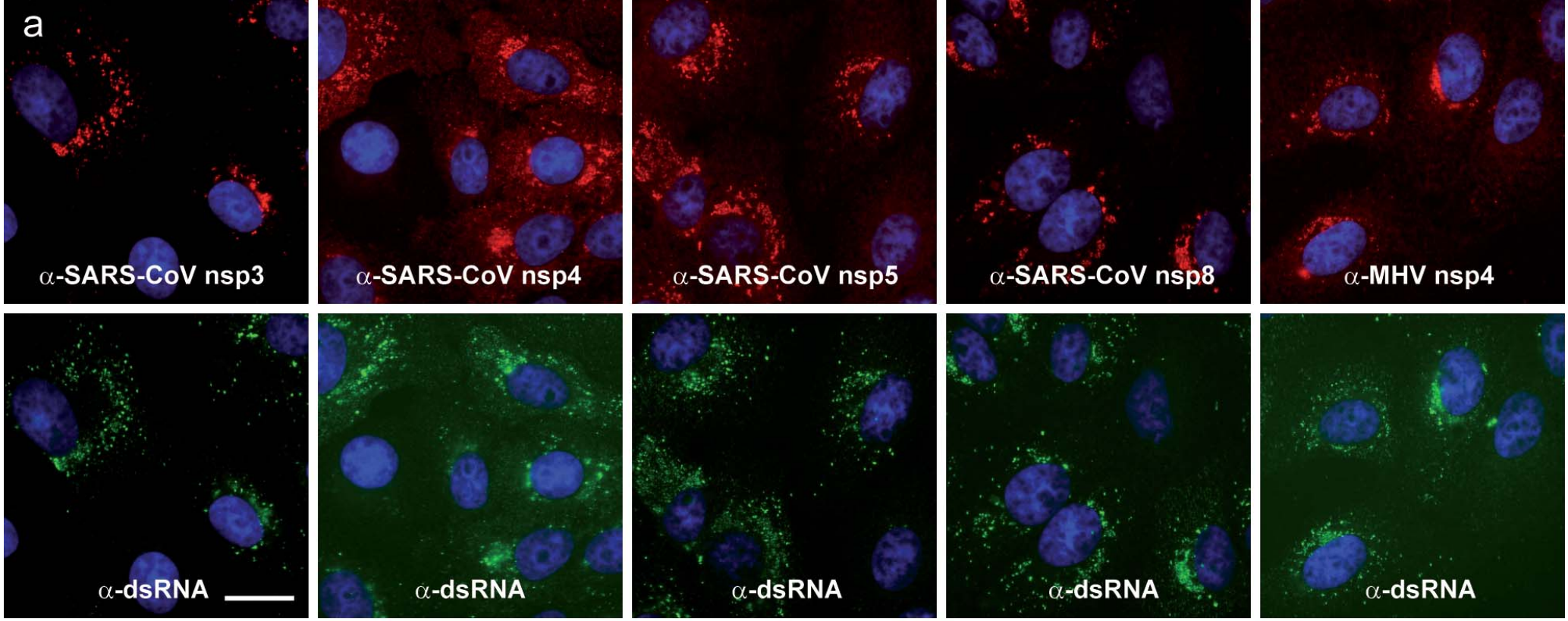

b

SARS-CoV pp1a	3218	FSNSGADVLYQPPQTSITSAVLQ	3240
MERS-CoV pp1a	3225	YSETGSDLLYQPPNCSITSGVLQ	3247
MHV-A59 pp1a	3311	NHNNGNDVLYQPPTASVTTSFLQ	3333

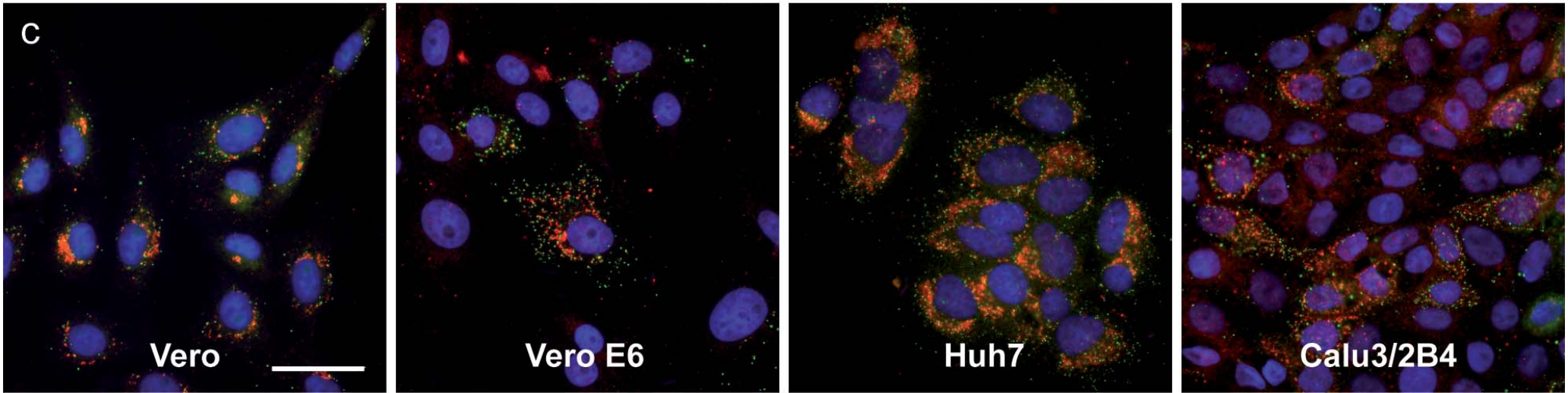

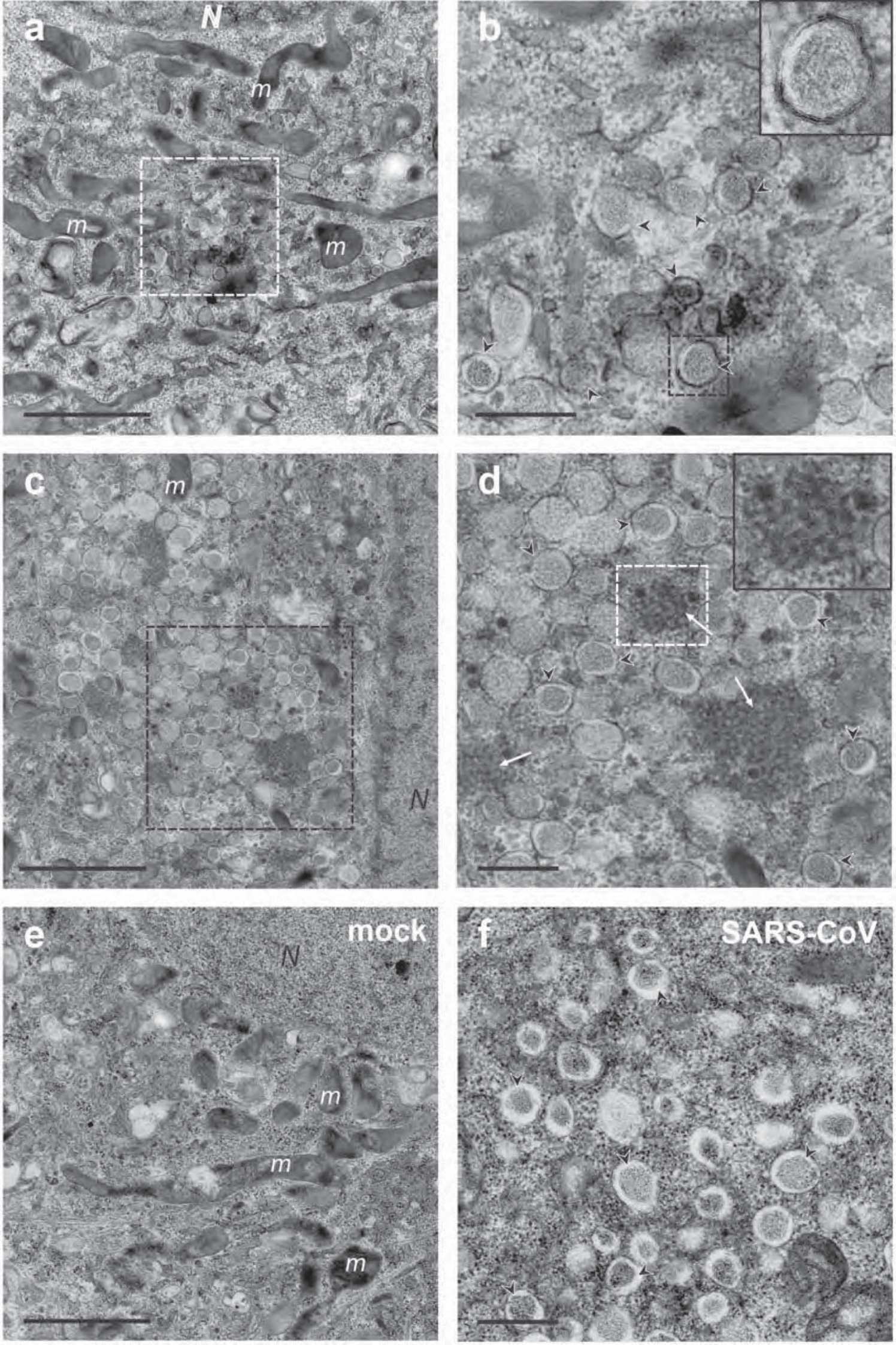
a
N
m
m
m
b
c
m
N
d
e
mock
N
m
m
m
f
SARS-CoV

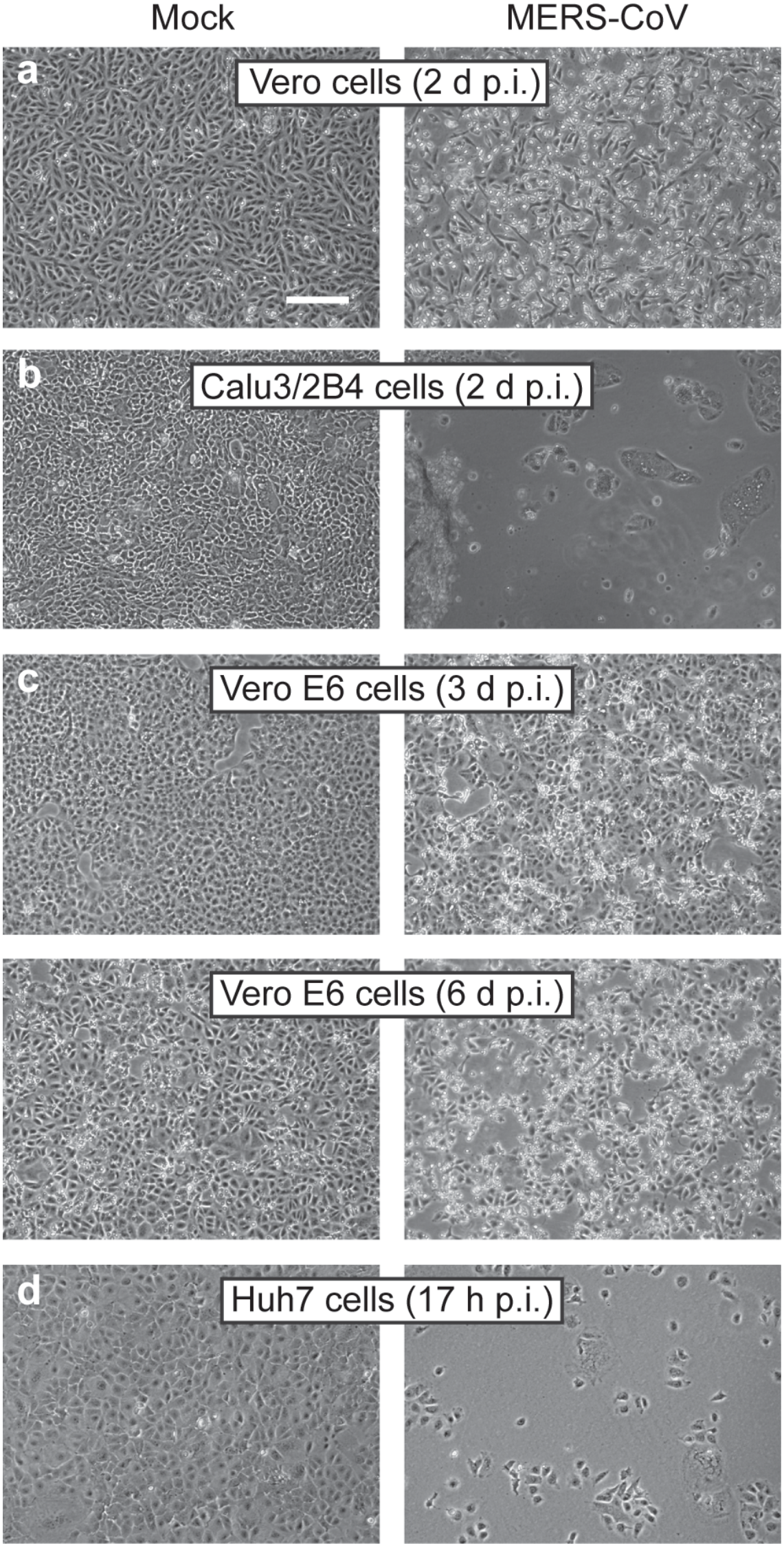
Mock
MERS-CoV
a
Vero cells (2 d p.i.)
b
Calu3/2B4 cells (2 d p.i.)
c
Vero E6 cells (3 d p.i.)
Vero E6 cells (6 d p.i.)
d
Huh7 cells (17 h p.i.)

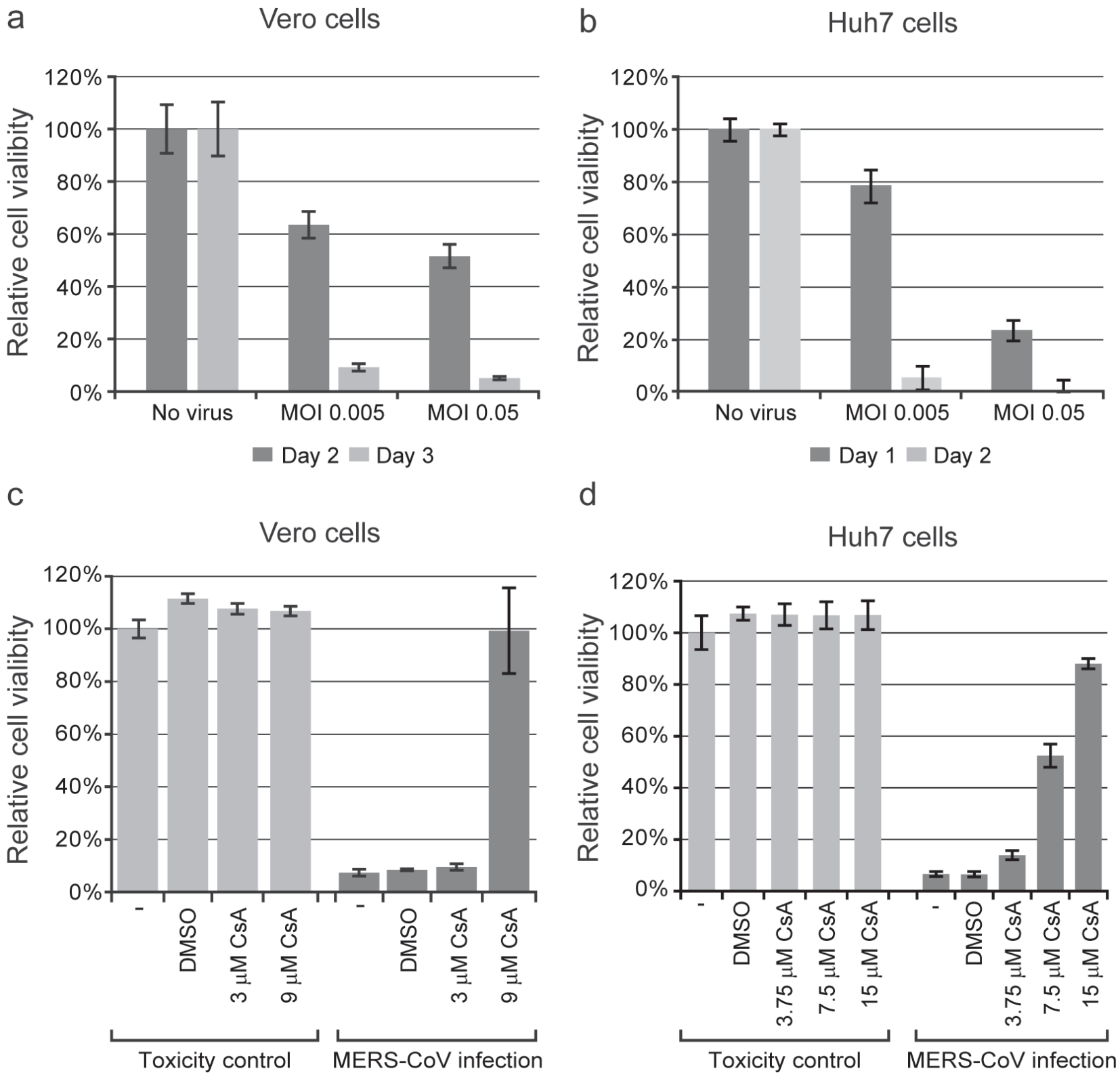
a
Vero cells
Relative cell vialibity
120%
100%
80%
60%
40%
20%
0%
No virus
MOI 0.005
MOI 0.05
Day 2
Day 3
b
Huh7 cells
Relative cell vialibity
120%
100%
80%
60%
40%
20%
0%
No virus
MOI 0.005
MOI 0.05
Day 1
Day 2
c
Vero cells
Relative cell vialibity
120%
100%
80%
60%
40%
20%
0%
-
DMSO
3 µM CsA
9 µM CsA
-
DMSO
3 µM CsA
9 µM CsA
Toxicity control
MERS-CoV infection
d
Huh7 cells
Relative cell vialibity
120%
100%
80%
60%
40%
20%
0%
-
DMSO
3.75 µM CsA
7.5 µM CsA
15 µM CsA
-
DMSO
3.75 µM CsA
7.5 µM CsA
15 µM CsA
Toxicity control
MERS-CoV infection

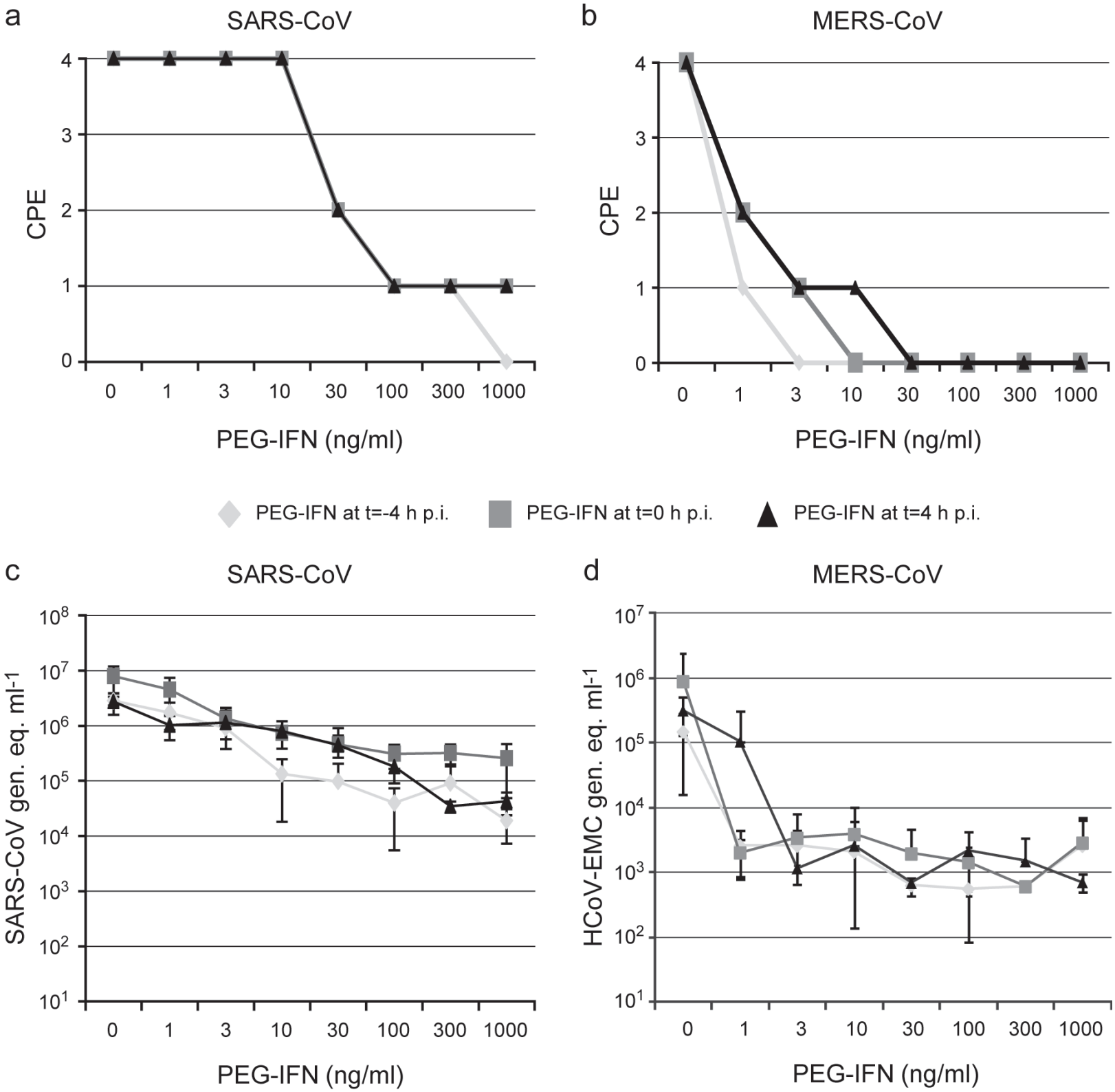
a
SARS-CoV
CPE
PEG-IFN (ng/ml)
b
MERS-CoV
CPE
PEG-IFN (ng/ml)
PEG-IFN at t=-4 h p.i.
PEG-IFN at t=0 h p.i.
PEG-IFN at t=4 h p.i.
c
SARS-CoV
SARS-CoV gen. eq. ml-1
PEG-IFN (ng/ml)
d
MERS-CoV
HCoV-EMC gen. eq. ml-1
PEG-IFN (ng/ml)

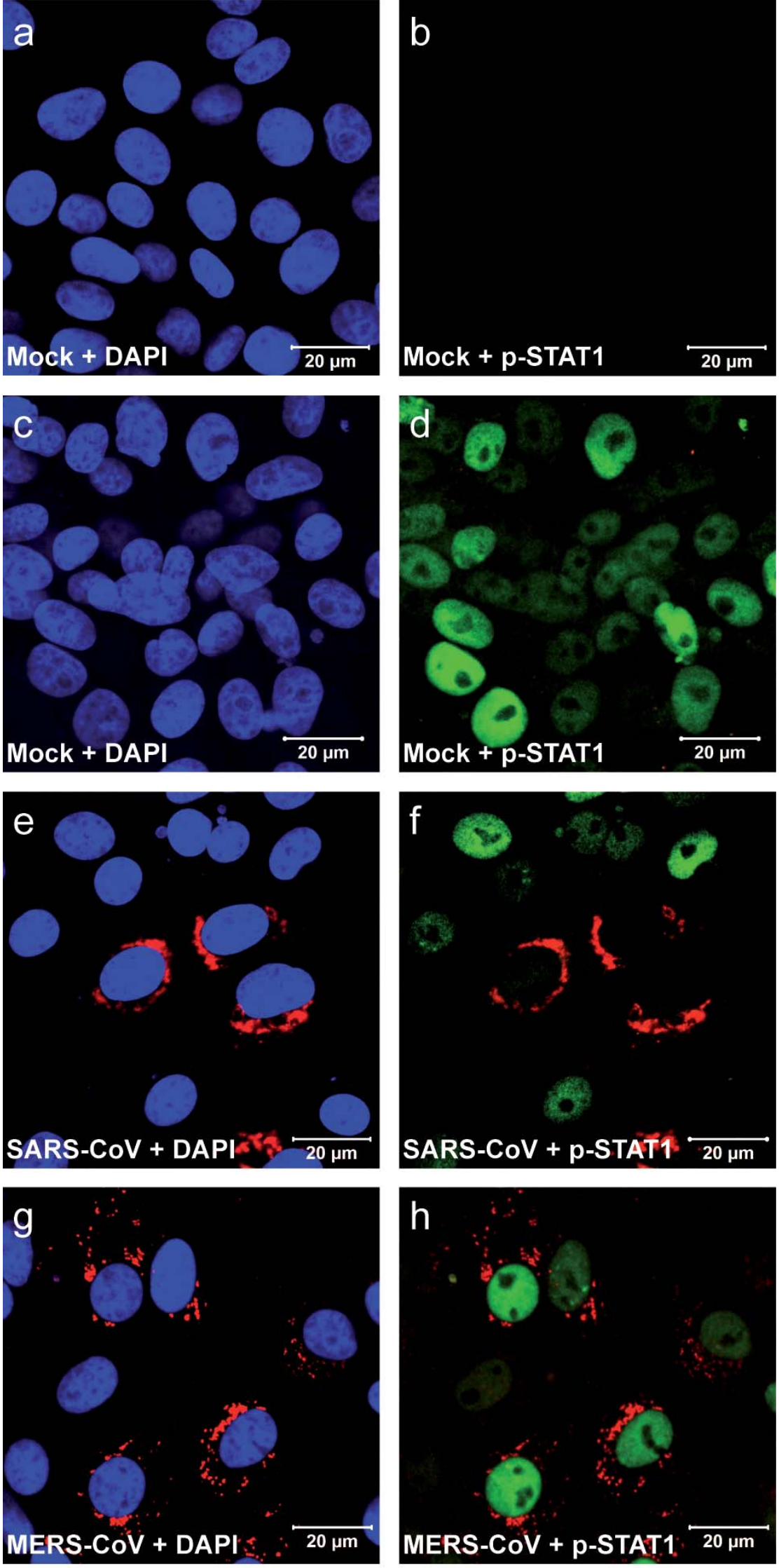
a
Mock + DAPI
20 µm
b
Mock + p-STAT1
20 µm
c
Mock + DAPI
20 µm
d
Mock + p-STAT1
20 µm
e
SARS-CoV + DAPI
20 µm
f
SARS-CoV + p-STAT1
20 µm
g
MERS-CoV + DAPI
20 µm
h
MERS-CoV + p-STAT1
20 µm